Characterization and Design of Three-Phase EMI Noise Separators for Three-Phase Power Electronics Systems

Shuo Wang, *Senior Member, IEEE*, Fang Luo, *Member, IEEE*, and Fred C. Lee, *Fellow, IEEE*

***Abstract*—In this paper, three-phase noise is first analyzed using symmetrical component theory. Three-phase noise separators are modeled and characterized using symmetrical component theory and S-parameters. The critical formulas used to evaluate a three-phase noise separator are derived. A function scheme and a circuit structure for three-phase noise separators are proposed based on the theory developed. The technique to design a high-performance three-phase noise separator is explored. A three-phase noise separator prototype is finally built, measured, and evaluated using the theory developed in this paper. The prototype is used in a practical three-phase power electronics system for electromagnetic interference measurement.**

***Index Terms*—Bifilar winding, common-mode rejection ratio (CMRR), common-mode transmission ratio (CMTR), differential-mode rejection ratio (DMRR), differential-mode transmission ratio (DMTR), electromagnetic interference (EMI), noise separator, scattering parameters, symmetrical component theory, three-phase, transmission line transformer, trifilar winding.**

I. Introduction

THREE-PHASE power electronics systems are very popular in high-power applications. However, because of the high currents, high-current ripples, high *dv/dt*, and large parasitic parameters in these power electronics systems, the electromagnetic interference (EMI) noise is hard to control. The size of the EMI filters can be significant. It may take up to half the size of the whole power electronics systems. Conventionally, EMI noise can be decoupled to differential-mode (DM) and common-mode (CM) noise. DM and CM filters are used to suppress DM and CM noises, respectively. How to optimize the EMI filter design so that its size can be minimized is an important research topic [1]. One of the approaches to optimize filter design is to design EMI filters based on the measured EMI noise. However, the conventional measurement method cannot differentiate DM and CM noises; as a result, the measurement results cannot effectively help engineers do an optimal filter design. This paper will first characterize three-phase noise separators using network theory. A three-phase noise separator is then proposed and designed. Experiments are carried out to evaluate the noise separator based on the developed theory. The designed noise separator is finally used in an EMI measurement for a practical three-phase power electronics system.

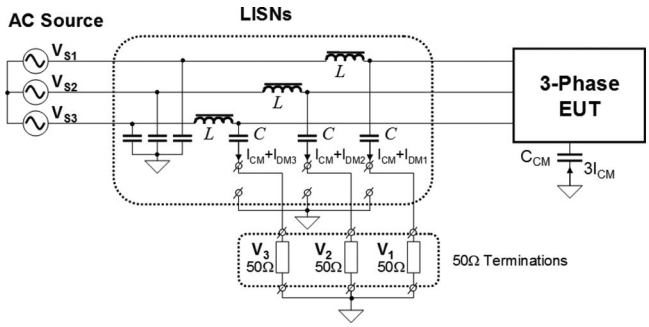

Fig. 1. EMI noise measurement setup for a three-phase power electronics system.

A typical EMI noise measurement setup for a three-phase power electronics system is shown in Fig. 1. Parasitic capacitances, especially the parasitic capacitance $C_{\rm CM}$ between the high *dv/dt* nodes and the ground, offer paths for CM noise. The CM noise $3\mathbf{I_{CM}}$ comes back to the system through 50-Ω terminations and line impedance stabilizing networks (LISNs). DM noises $\mathbf{I_{DM1}}$, $\mathbf{I_{DM2}}$, and $\mathbf{I_{DM3}}$ also flow through LISNs and 50-Ω terminations. Here, 50-Ω terminations can either be the input impedances of a spectrum analyzer or standard 50-Ω terminators. The DM or CM noise voltage drops on a 50-Ω resistance are defined as DM or CM noise voltages.

In Fig. 1, the noise voltage drop $\mathbf{V_1}$, $\mathbf{V_2}$, or $\mathbf{V_3}$ on one of the 50-Ω terminations is defined as the total noise on phases 1, 2, or 3, and it is the vector sum of CM and DM noise voltages on each phase. The CM and DM noise voltages can then be calculated as

$$|\mathbf{V_{CM}}| = \left|\frac{\mathbf{V}_1+\mathbf{V}_2+\mathbf{V}_3}{3}\right| = 50\,|\mathbf{I_{CM}}| \tag{1}$$

$$|\mathbf{V_{DM1}}| = |\mathbf{V}_1-\mathbf{V_{CM}}| = \left|\frac{2\mathbf{V}_1-\mathbf{V}_2-\mathbf{V}_3}{3}\right| = 50\,|\mathbf{I_{DM1}}| \tag{2}$$

Manuscript received October 5, 2010; revised December 19, 2010 and December 31, 2010; accepted January 2, 2011. Date of current version September 16, 2011. Recommended for publication by Associate Editor R. Redl.

S. Wang is with the Department of Electrical and Computer Engineering, University of Texas at San Antonio, San Antonio, TX 78249 USA (e-mail: shuowang@ieee.org).

F. Luo is with the Center for Power Electronics Systems (CPES), Virginia Tech, Blacksburg, VA 24061 USA (e-mail: fangluo@vt.edu).

F. C. Lee is with the Department of Electrical and Computer Engineering, Virginia Tech, Blacksburg, VA 24061 USA (e-mail: fclee@vt.edu).

Color versions of one or more of the figures in this paper are available online at http://ieeexplore.ieee.org.

Digital Object Identifier 10.1109/TPEL.2011.2106224

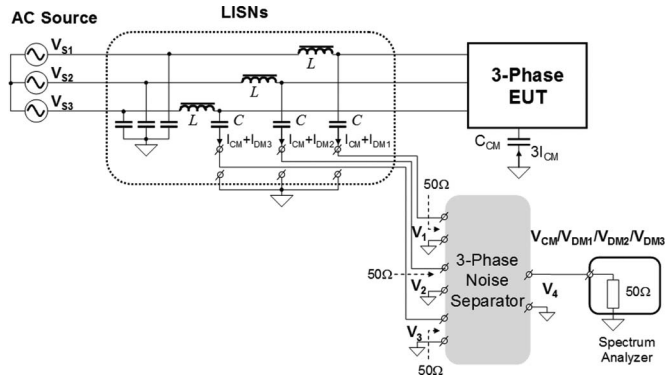

Fig. 2. Using a three-phase noise separator to separate DM and CM noises.

$$|\mathbf{V}_{\mathrm{DM}2}| = |\mathbf{V}_2 - \mathbf{V}_{\mathrm{CM}}| = \left|\frac{2\mathbf{V}_2 - \mathbf{V}_1 - \mathbf{V}_3}{3}\right| = 50\,|\mathbf{I}_{\mathrm{DM}2}| \tag{3}$$

$$|\mathbf{V}_{\mathrm{DM}3}| = |\mathbf{V}_3 - \mathbf{V}_{\mathrm{CM}}| = \left|\frac{2\mathbf{V}_3 - \mathbf{V}_1 - \mathbf{V}_2}{3}\right| = 50\,|\mathbf{I}_{\mathrm{DM}3}|\,. \tag{4}$$

Fig. 2 shows an EMI noise measurement setup with a three-phase noise separator. There are three input ports and one output port. Three input ports have 50-Ω input impedances terminating LISNs. Output is terminated by the 50-Ω input impedance of a spectrum analyzer. The output of the noise separator could be the CM noise V_{CM}, phase 1 DM noise $V_{\mathrm{DM}1}$, phase 2 DM noise $V_{\mathrm{DM}2}$, or phase 3 DM noise $V_{\mathrm{DM}3}$.

In order to separate DM and CM noises, the noise separator should satisfy three requirements.

1) Input impedances are always real 50 Ω and are independent from noise source impedances.
2) The output of the CM noise is $|(\mathbf{V_1} + \mathbf{V_2} + \mathbf{V_3})/3|$, the output of the DM noise for phase 1 is $|(2\mathbf{V_1} - \mathbf{V_2} - \mathbf{V_3})/3|$, for phase 2 is $|(2\mathbf{V_2} - \mathbf{V_1} - \mathbf{V_3})/3|$, and for phase 3 is $|(2\mathbf{V_3} - \mathbf{V_1} - \mathbf{V_2})/3|$.
3) Leakage between the CM and the DM at the output should be small.

The requirement: 1) guarantees consistent measurement conditions and accurate sampling of noise voltage; 2) guarantees correct noise separation; and 3) guarantees small interference between the CM and DM noise measurements.

The first requirement can be characterized using network parameters, such as the reflection coefficient in wave theory. The second requirement can be characterized by the transmission coefficient of noise separators. The DM transmission ratio (DMTR) for the DM noise separator and the CM transmission ratio (CMTR) for the CM noise separator are two parameters that need to be characterized and evaluated. They have been defined and discussed in [2] for two-phase noise separators as follows.

For a CM noise separator

$$\mathrm{CMTR} = \left|\frac{\mathbf{V}_{\mathbf{CM\_out}}}{\mathbf{V}_{\mathbf{CM\_in}}}\right|. \tag{5}$$

For a DM noise separator

$$\mathrm{DMTR} = \left|\frac{\mathbf{V}_{\mathbf{DM\_out}}}{\mathbf{V}_{\mathbf{DM\_in}}}\right|. \tag{6}$$

In (5), $\mathbf{V}_{\mathbf{CM\_in}}$ is the CM voltage excitation fed to the inputs of a CM noise separator. The CM voltage excitation added to each input port. $\mathbf{V}_{\mathbf{CM\_out}}$ is the voltage response at the output of this CM noise separator due to $\mathbf{V}_{\mathbf{CM\_in}}$. In (6), $\mathbf{V}_{\mathbf{DM\_in}}$ is the DM voltage excitation fed to the inputs of a DM noise separator. $\mathbf{V}_{\mathbf{DM\_out}}$ is the voltage response at the output of this DM noise separator due to $\mathbf{V}_{\mathbf{DM\_in}}$. From (5) and (6), the ideal CMTR and DMTR should be 0 dB. Different from two-phase DM noise separators, a three-phase DM noise separator has two different DMTRs for each phase. This will be discussed in detail in Section II.

The third requirement can be characterized by two parameters: the DM rejection ratio (DMRR) and the CM rejection ratio (CMRR). They have been defined and discussed in [2] for two-phase noise separators as follows.

For a CM noise separator

$$\mathrm{DMRR} = \left|\frac{\mathbf{V}_{\mathbf{CM\_out}}}{\mathbf{V}_{\mathbf{DM\_in}}}\right| \quad \text{and} \tag{7}$$

for a DM noise separator

$$\mathrm{CMRR} = \left|\frac{\mathbf{V}_{\mathbf{DM\_out}}}{\mathbf{V}_{\mathbf{CM\_in}}}\right| \tag{8}$$

where $\mathbf{V}_{\mathbf{DM\_in}}$ is the DM voltage excitation fed to the inputs of a CM noise separator, $\mathbf{V}_{\mathbf{CM\_out}}$ is the voltage response at the output of this CM noise separator due to $\mathbf{V}_{\mathbf{DM\_in}}$. $\mathbf{V}_{\mathbf{CM\_in}}$ is the CM voltage fed to the inputs of a DM noise separator, and $\mathbf{V}_{\mathbf{DM\_out}}$ is the output voltage of this DM noise separator due to $\mathbf{V}_{\mathbf{CM\_in}}$. DMRR and CMRR should be as small as possible. On the other hand, a three-phase DM noise separator has a CMRR for each phase and a three-phase CM noise separator has two different DMRRs. This will be discussed in detail in Section II.

Appropriate network parameters need to be introduced to characterize and evaluate noise separators using the three requirements. Scattering parameters (S-parameters) are selected in this paper because of three reasons. First, frequency-domain characterization of network employing ***[Z]***, ***[Y]***, ***[H]***, and ***[ABCD]*** parameters often requires either a short circuit or an open circuit at one port, which is difficult to achieve in the high frequency (HF) range because of parasitic parameters [3], [4]. On the other hand, for S-parameters, no short or open circuit is needed. Second, S-parameter method can be calibrated to the exact points of measurement, so that the effects of parasitics due to measurement interconnects are excluded. For ***[Z]***, ***[Y]***, ***[H]***, and ***[ABCD]*** parameters measurement, expensive special probes may be needed for calibration. Third, S-parameters are analytically convenient and capable of providing a great insight into a measurement or design problem [4]. Thanks to S-parameters, the powerful signal flow graph can be used for network analysis with clear physical concepts.

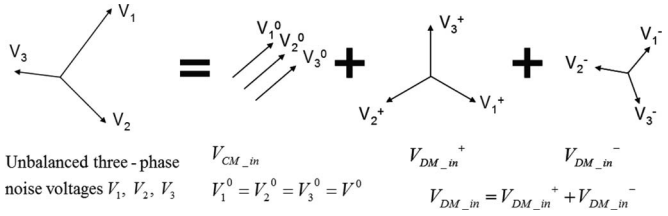

Fig. 3. Unbalanced three-phase noise voltage is decomposed to CM, positive and negative sequence DM voltages.

II. Characterization of Three-Phase Noise Separators

This section will first discuss the transmission and rejection ratios for three-phase noise separators. The three-phase noise separator is then characterized using S-parameters. The transmission and rejection ratios are finally derived using S-parameters.

A. Transmission and Rejection Ratios of a Three-phase Noise Separator

Similar to two-phase noise separators, three-phase and multiphase noise separators can also be evaluated using transmission and reflection ratios. For the three-phase noise separator in Fig. 2, the three-phase noise voltage set added to the input ports has 6 DOF because the magnitude and phase of each phase are independent from others. Because of this, the parameters used to characterize a three-phase noise voltage set must have 6 DOF. Based on symmetrical component theory, an unbalanced three-phase voltage set can be decomposed to a zero-sequence voltage set V^0, V^0, V^0; a positive sequence voltage set, V_1^+, V_2^+, V_3^+; and a negative sequence voltage set, V_1^-, V_2^-, V_3^-. Each set has 2 DOF so there are 6 DOF in total. The symmetrical component theory is applied to the three-phase noise analysis in (9). The CM and DM noises added to the input ports of the three-phase noise separator are represented with zero, positive, and negative sequence voltage sets in (10) and (11). From (10), the CM noise voltage is the same as zero-sequence noise voltage. From (11), the DM noise of each phase is the sum of the positive sequence and negative sequence noise voltages. The relationship can be shown in Fig. 3, where $V_{\mathrm{DM\_in}}^+$ and $V_{\mathrm{DM\_in}}^-$ are positive and negative sequence voltage sets

$$\begin{pmatrix} V_1 \\ V_2 \\ V_3 \end{pmatrix} = \begin{pmatrix} V^0 \\ V^0 \\ V^0 \end{pmatrix} + \begin{pmatrix} V_1^+ \\ V_2^+ \\ V_3^+ \end{pmatrix} + \begin{pmatrix} V_1^- \\ V_2^- \\ V_3^- \end{pmatrix} \tag{9}$$

$$V_{\mathrm{CM\_in}} = \frac{V_1 + V_2 + V_3}{3} = V^0 \tag{10}$$

$$\begin{pmatrix} V_{\mathrm{DM1\_in}} \\ V_{\mathrm{DM2\_in}} \\ V_{\mathrm{DM3\_in}} \end{pmatrix} = \begin{pmatrix} V_1 \\ V_2 \\ V_3 \end{pmatrix} - \begin{pmatrix} V_{\mathrm{CM\_in}} \\ V_{\mathrm{CM\_in}} \\ V_{\mathrm{CM\_in}} \end{pmatrix} = \begin{pmatrix} V_1^+ \\ V_2^+ \\ V_3^+ \end{pmatrix} + \begin{pmatrix} V_1^- \\ V_2^- \\ V_3^- \end{pmatrix}. \tag{11}$$

The CM or DM output of a three-phase noise separator can be calculated as

$$V_{\mathrm{CM\_out}} = \mathrm{CMTR} \times V_{\mathrm{CM\_in}} \tag{12}$$

$$\begin{pmatrix} V_{\mathrm{DM1\_out}} \\ V_{\mathrm{DM2\_out}} \\ V_{\mathrm{DM3\_out}} \end{pmatrix} = \begin{pmatrix} \mathrm{DMTR}_1^+ \times V_1^+ \\ \mathrm{DMTR}_2^+ \times V_2^+ \\ \mathrm{DMTR}_3^+ \times V_3^+ \end{pmatrix} + \begin{pmatrix} \mathrm{DMTR}_1^- \times V_1^- \\ \mathrm{DMTR}_2^- \times V_2^- \\ \mathrm{DMTR}_3^- \times V_3^- \end{pmatrix}. \tag{13}$$

In (12), CMTR is the CM transmission ratio. In (13), because positive and negative sequences are independent from each other, each phase has a positive sequence transmission ratio and a negative sequence transmission ratio.

Based on (12), the CMTR for a CM noise separator can be calculated as

$$\mathrm{CMTR} = \left.\frac{V_{\mathrm{CM\_out}}}{V_{\mathrm{CM\_in}}}\right|_{V_{\mathrm{DM\_in}}^+ = 0, V_{\mathrm{DM\_in}}^- = 0}. \tag{14}$$

Based on (13), the DMTR for a DM noise separator can be calculated as

$$\mathrm{DMTR}_n^+ = \left.\frac{V_{\mathrm{DM}n\_\mathrm{out}}}{V_n^+}\right|_{V_{\mathrm{DM\_in}}^- = 0, V_{\mathrm{CM\_in}} = 0} \tag{15}$$

$$\mathrm{DMTR}_n^- = \left.\frac{V_{\mathrm{DM}n\_\mathrm{out}}}{V_n^-}\right|_{V_{\mathrm{DM\_in}}^+ = 0, V_{\mathrm{CM\_in}} = 0}. \tag{16}$$

In (15) and (16), n is the phase number from 1 to 3. In (15), a positive sequence voltage set is fed to the noise separator while a negative sequence set and CM voltage are zero. In (16), a negative sequence voltage set is fed to the noise separator while a positive sequence set and CM voltage are zero. Because the outputs of a DM noise separator are the vector sum of positive and negative sequence voltage responses, both magnitudes and phases of DMTR_n^+ and DMTR_n^- are important. Ideally, both magnitudes should be 0 dB and two phases should be same. On the other hand, the phase of CMTR is not so important because only its magnitude is read on the spectrum analyzer. An ideal CMTR should be equal to 0 dB.

Similarly, a CM noise separator has a positive sequence DMRR and a negative sequence DMRR

$$\mathrm{DMRR}^+ = \left.\frac{V_{\mathrm{CM\_out}}}{V_1^+}\right|_{V_{\mathrm{DM\_in}}^- = 0, V_{\mathrm{CM\_in}} = 0} \tag{17}$$

$$\mathrm{DMRR}^- = \left.\frac{V_{\mathrm{CM\_out}}}{V_1^-}\right|_{V_{\mathrm{DM\_in}}^+ = 0, V_{\mathrm{CM\_in}} = 0}. \tag{18}$$

In (17), a positive sequence voltage set is fed to the noise separator while a negative sequence set and CM voltage are zero. In (18), a negative sequence voltage set is fed to the noise separator while a positive sequence set and CM voltage are zero. Both DMRRs should be as small as possible. When they are much smaller than 0 dB, their phases are not important.

Each phase of a DM noise separator has a CMRR

$$\mathrm{CMRR}_n = \left.\frac{V_{\mathrm{DM}n\_\mathrm{out}}}{V_{\mathrm{CM\_in}}}\right|_{V_{\mathrm{DM\_in}}^+ = 0, V_{\mathrm{DM\_in}}^- = 0}. \tag{19}$$

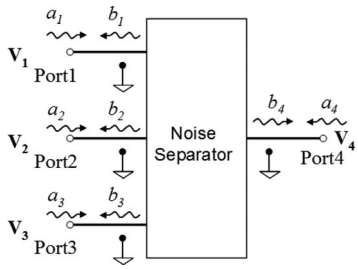

Fig. 4. Characterizing a three-phase noise separator in terms of waves.

In (19), n is the phase number from 1 to 3. CMRR should be as small as possible and its phase is not important since only its magnitude is read on the spectrum analyzer.

It should be pointed out that because the DM noise added to the noise separator has 4 DOF; any methods using an excitation with 2 DOF cannot offer a full evaluation for DMTR and DMRR.

B. Characterization of a Noise Separator Using S-Parameters

For a CM or DM three-phase noise separator in Fig. 2, there are three input ports port1, port2, and port3 and one output port port4, so it is a four-port network. This four-port linear passive network can be characterized in terms of waves, as shown in Fig. 4.

In Fig. 4, a_n is the normalized incident wave, and b_n is the normalized reflected wave. Port voltage $\mathbf{V_n}$ can be expressed as follows [5], [6]:

$$\mathbf{V_n} = \sqrt{Z_0}(a_n + b_n) \tag{20}$$

where Z_0 is the reference impedance, which is usually 50 Ω, and n is the port number.

To fully characterize a four-port linear passive network, four linear equations are required among the eight wave variables [11]. The sixteen S-parameters in (21) are, therefore, introduced to correlate a_n and b_n [5], [7]. S_{nn} refers to the reflection coefficients, and S_{mn} represents the transmission coefficients. Both m and n are port numbers

$$\begin{pmatrix} b_1 \\ b_2 \\ b_3 \\ b_4 \end{pmatrix} = \begin{pmatrix} S_{11} & S_{12} & S_{13} & S_{14} \\ S_{21} & S_{22} & S_{23} & S_{24} \\ S_{31} & S_{32} & S_{33} & S_{34} \\ S_{41} & S_{42} & S_{43} & S_{44} \end{pmatrix} \begin{pmatrix} a_1 \\ a_2 \\ a_3 \\ a_4 \end{pmatrix} \Rightarrow [\mathbf{b}] = [\mathbf{S}]\,[\mathbf{a}]\,. \tag{21}$$

According to the transmission-line theory [5], [8], when reflected wave b_n reaches the source or load side, it will also be reflected because of the mismatched impedances. The reflection coefficients Γ_{sn} at source side and Γ_L at load side are given through (22) and (23). It is known that for passive networks, $|\Gamma_{sn}| \le 1$ and $|\Gamma_L| \le 1$

$$\Gamma_{sn} = \frac{\mathrm{Z}_{sn} - Z_0}{Z_{sn} + Z_0} \tag{22}$$

and

$$\Gamma_L = \frac{Z_L - Z_0}{Z_L + Z_0}. \tag{23}$$

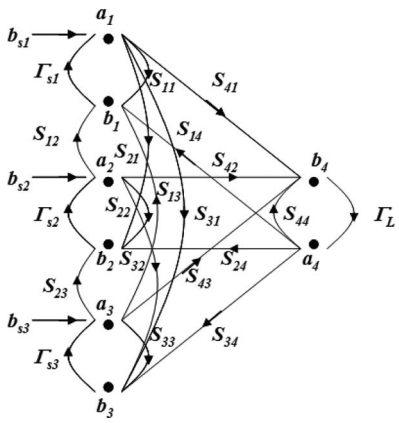

Fig. 5. Characterizing the noise separator using a signal flow graph.

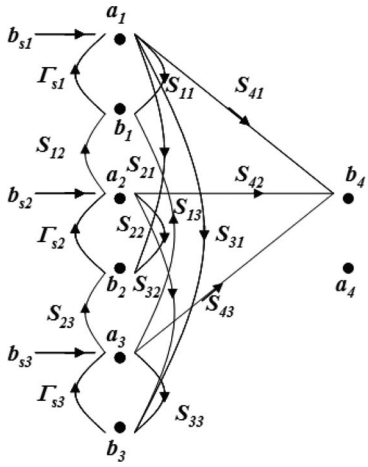

Fig. 6. Signal-flow graph for a practical noise separator with a matched load at port4.

Fig. 4 is then characterized by the signal flow graph in Fig. 5. In Fig. 5, b_{sn} is the normalized wave emanating from the source. For a given voltage source $\mathbf{V_{sn}}$ with source impedance Z_{sn}, b_{sn} is given as follows [8]:

$$b_{sn} = \frac{\sqrt{Z_0}\mathbf{V_{sn}}}{Z_{sn} + Z_0}. \tag{24}$$

Because the output of the noise separator is terminated by the 50-Ω input impedance of the spectrum analyzer, which is shown in Fig. 2, the reflection coefficient Γ_L is zero. As a result, a_4 is zero, and the signal-flow graph is equivalent to Fig. 6. Fig. 6 characterizes a practical noise separator matched by a spectrum analyzer at port4. It is now important to determine the appropriate $\mathbf{S}$ matrix for an ideal noise separator.

In order to achieve 50-Ω input impedance independent from noise source impedance, the reflection coefficients at port1, port2, and port3 must be zero. In Fig. 6, by using Mason's rule, the reflection coefficients Γ_1, Γ_2, and Γ_3 for port1, port2, and port3 are described, as shown (25)–(27), at the bottom of the next page, where $Z_{\mathrm{in}1}$, $Z_{\mathrm{in}2}$, and $Z_{\mathrm{in}3}$ are the input impedances of port1, port2, and port3, respectively. Δ_1, Δ_2, and Δ_3 represent the second terms in (25), (26), and (27), respectively.

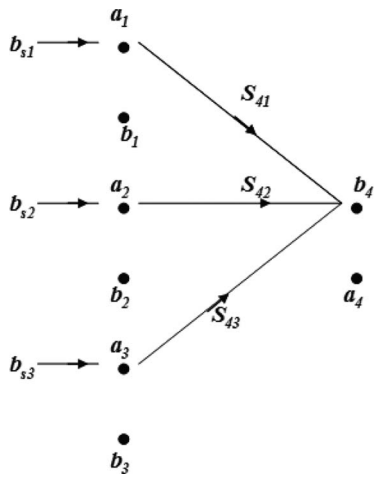

Fig. 7. Signal-flow graph for an ideal three-phase noise separator with a matched load at port4.

From (25), (26), and (27), in order to guarantee a 50-Ω input impedance independent from noise source impedance, S_{11}, S_{22}, S_{33} and S_{12}, S_{21}, S_{13}, S_{31}, S_{32}, S_{23} must be zero; as a result, b_1, b_2, and b_3 are zero. The signal-flow graph is, thus, equivalent to Fig. 7.

In Fig. 7, based on (20), the voltage at port4 is given by

$$\mathbf{V_4} = \mathbf{V_1} S_{41} + \mathbf{V_2} S_{42} + \mathbf{V_3} S_{43}. \tag{28}$$

Based on (1)–(4), and (28), for a CM noise separator

$$S_{41} = S_{42} = S_{43} = \frac{1}{3}, \quad \text{or} \quad S_{41} = S_{42} = S_{43} = -\frac{1}{3}. \tag{29}$$

For the DM noise separator of phase 1

$$S_{41} = \frac{2}{3}, \quad S_{42} = -\frac{1}{3}, \quad S_{43} = -\frac{1}{3}, \quad \text{or}$$
$$S_{41} = -\frac{2}{3}, \quad S_{42} = \frac{1}{3}, \quad S_{43} = \frac{1}{3}. \tag{30}$$

For the DM noise separator of phase 2

$$S_{41} = -\frac{1}{3}, \quad S_{42} = \frac{2}{3}, \quad S_{43} = -\frac{1}{3}, \quad \text{or}$$
$$S_{41} = \frac{1}{3}, \quad S_{42} = -\frac{2}{3}, \quad S_{43} = \frac{1}{3}. \tag{31}$$

For the DM noise separator of phase 3

$$S_{41} = -\frac{1}{3}, \quad S_{42} = -\frac{1}{3}, \quad S_{43} = \frac{2}{3}, \quad \text{or}$$
$$S_{41} = \frac{1}{3}, \quad S_{42} = \frac{1}{3}, \quad S_{43} = -\frac{2}{3}. \tag{32}$$

The final $\mathbf{S}$ matrix for an ideal CM noise separator is therefore

$$[\mathbf{S}] = \begin{pmatrix} 0 & 0 & 0 & S_{14} \\ 0 & 0 & 0 & S_{24} \\ 0 & 0 & 0 & S_{34} \\ \pm\frac{1}{3} & \pm\frac{1}{3} & \pm\frac{1}{3} & S_{44} \end{pmatrix}. \tag{33}$$

The $\mathbf{S}$ matrix for the ideal DM noise separator of phase 1

$$[\mathbf{S}] = \begin{pmatrix} 0 & 0 & 0 & S_{14} \\ 0 & 0 & 0 & S_{24} \\ 0 & 0 & 0 & S_{34} \\ \pm\frac{2}{3} & \mp\frac{1}{3} & \mp\frac{1}{3} & S_{44} \end{pmatrix}. \tag{34}$$

The $\mathbf{S}$ matrix for the ideal DM noise separator of phase 2

$$[\mathbf{S}] = \begin{pmatrix} 0 & 0 & 0 & S_{14} \\ 0 & 0 & 0 & S_{24} \\ 0 & 0 & 0 & S_{34} \\ \mp\frac{1}{3} & \pm\frac{2}{3} & \mp\frac{1}{3} & S_{44} \end{pmatrix}. \tag{35}$$

The $\mathbf{S}$ matrix for the ideal DM noise separator of phase 3

$$[\mathbf{S}] = \begin{pmatrix} 0 & 0 & 0 & S_{14} \\ 0 & 0 & 0 & S_{24} \\ 0 & 0 & 0 & S_{34} \\ \mp\frac{1}{3} & \mp\frac{1}{3} & \pm\frac{2}{3} & S_{44} \end{pmatrix}. \tag{36}$$

In (33)–(35), and (36), the fourth column in the $\mathbf{S}$ matrix has nothing to do with the performance of a noise separator because port4 is matched. Therefore, there is no output impedance requirement. For a noise separator, S_{11}, S_{22}, S_{33} and S_{12}, S_{21}, S_{13}, S_{31}, S_{32}, S_{23} should be as small as possible. S_{41}, S_{42}, and S_{43} should be $\pm 1/3$ for a CM noise separator. For a DM noise separator, S_{41}, S_{42}, and S_{43} should be $\pm 2/3$, $\mp 1/3$, $\mp 1/3$ for phase 1; $\mp 1/3$, $\pm 2/3$, $\mp 1/3$ for phase 2; and $\mp 1/3$, $\mp 1/3$, $\pm 2/3$ for phase 3.

For a practical noise separator, S_{11}, S_{22}, S_{33} and S_{12}, S_{21}, S_{13}, S_{31}, S_{32}, S_{23} are not zero; and S_{41}, S_{42}, and S_{43} are not exactly equal to the values defined in (34), (35), and (36) too, so Fig. 6 should be used for evaluation. The input impedance of a noise separator can be evaluated through (25), (26), and (27). In (25), (26), and (27), the second term can be ignored if it is much smaller than the first term. This means that input impedances are independent from Γ_{s1}, Γ_{s2}, and Γ_{s3}, which represent the source impedances. Then, the input impedances

$$\Gamma_1 = \frac{Z_{\text{in}1} - Z_0}{Z_{\text{in}1} + Z_0} = S_{11} + \frac{S_{21}\Gamma_{s2}S_{12}(1 - S_{33}\Gamma_{s3}) + S_{31}\Gamma_{s3}S_{13}(1 - S_{22}\Gamma_{s2}) + S_{31}\Gamma_{s3}S_{23}\Gamma_{s2}S_{12}}{1 - S_{22}\Gamma_{s2} - S_{33}\Gamma_{s3} - S_{32}\Gamma_{s3}S_{23}\Gamma_{s2} + S_{22}\Gamma_{s2}S_{33}\Gamma_{s3}} = S_{11} + \Delta_1 \tag{25}$$

$$\Gamma_2 = \frac{Z_{\text{in}2} - Z_0}{Z_{\text{in}2} + Z_0} = S_{22} + \frac{S_{12}\Gamma_{s1}S_{21}(1 - S_{33}\Gamma_{s3}) + S_{32}\Gamma_{s3}S_{23}(1 - S_{11}\Gamma_{s1}) + S_{32}\Gamma_{s3}S_{13}\Gamma_{s1}S_{21}}{1 - S_{11}\Gamma_{s1} - S_{33}\Gamma_{s3} - S_{31}\Gamma_{s3}S_{13}\Gamma_{s1} + S_{11}\Gamma_{s1}S_{33}\Gamma_{s3}} = S_{22} + \Delta_2 \tag{26}$$

$$\Gamma_3 = \frac{Z_{\text{in}3} - Z_0}{Z_{\text{in}3} + Z_0} = S_{33} + \frac{S_{23}\Gamma_{s2}S_{32}(1 - S_{11}\Gamma_{s1}) + S_{13}\Gamma_{s1}S_{31}(1 - S_{22}\Gamma_{s2}) + S_{13}\Gamma_{s1}S_{21}\Gamma_{s2}S_{32}}{1 - S_{11}\Gamma_{s1} - S_{22}\Gamma_{s2} - S_{12}\Gamma_{s1}S_{21}\Gamma_{s2} + S_{11}\Gamma_{s1}S_{22}\Gamma_{s2}} = S_{33} + \Delta_3 \tag{27}$$

can be characterized solely by S_{11}, S_{22}, and S_{33}, and are free of noise source impedances (37), (38), and (39) as follows:

$$Z_{\text{in1}} \approx Z_0 \frac{1+S_{11}}{1-S_{11}} \tag{37}$$

$$Z_{\text{in2}} \approx Z_0 \frac{1+S_{22}}{1-S_{22}} \tag{38}$$

and

$$Z_{\text{in3}} \approx Z_0 \frac{1+S_{33}}{1-S_{33}}. \tag{39}$$

Based on (14), (20), and Fig. 6, the CMTR for the CM noise separator can be derived using Mason's rule in (40), where the approximately equal values hold if the third term is much smaller than the second term in the denominators. This is also the condition for independent real 50-Ω input impedances in (37), (38), and (39). For a CM noise separator

$$\begin{aligned}\text{CMTR} = {} & \frac{S_{41}}{(1+S_{11}+\Delta_1)} + \frac{S_{42}}{(1+S_{22}+\Delta_2)} \\ & + \frac{S_{43}}{(1+S_{33}+\Delta_3)} \approx \frac{S_{41}}{(1+S_{11})} + \frac{S_{42}}{(1+S_{22})} \\ & + \frac{S_{43}}{(1+S_{33})}.\end{aligned} \tag{40}$$

For a good CM noise separator, the magnitude of CMTR should be close to 0 dB.

Based on (15), (16), (20), and Fig. 6, the DMTR_n^+ and DMTR_n^- for a DM noise separator can be derived using Mason's rule in (41)–(45), and (46).

For the DM noise separator of phase 1

$$\begin{aligned}\text{DMTR}^+ = {} & \frac{S_{41}}{(1+S_{11}+\Delta_1)} + \frac{S_{42}}{(1+S_{22}+\Delta_2)} \cdot e^{-j120^\circ} \\ & + \frac{S_{43}}{(1+S_{33}+\Delta_3)} \cdot e^{-j240^\circ}\end{aligned} \tag{41}$$

$$\begin{aligned}\text{DMTR}^- = {} & \frac{S_{41}}{(1+S_{11}+\Delta_1)} + \frac{S_{42}}{(1+S_{22}+\Delta_2)} \cdot e^{j120^\circ} \\ & + \frac{S_{43}}{(1+S_{33}+\Delta_3)} \cdot e^{j240^\circ}.\end{aligned} \tag{42}$$

For the DM noise separator of phase 2

$$\begin{aligned}\text{DMTR}^+ = {} & \frac{S_{41}}{(1+S_{11}+\Delta_1)} \cdot e^{j120^\circ} + \frac{S_{42}}{(1+S_{22}+\Delta_2)} \\ & + \frac{S_{43}}{(1+S_{33}+\Delta_3)} \cdot e^{-j120^\circ}\end{aligned} \tag{43}$$

$$\begin{aligned}\text{DMTR}^- = {} & \frac{S_{41}}{(1+S_{11}+\Delta_1)} \cdot e^{-j120^\circ} + \frac{S_{42}}{(1+S_{22}+\Delta_2)} \\ & + \frac{S_{43}}{(1+S_{33}+\Delta_3)} \cdot e^{j120^\circ}.\end{aligned} \tag{44}$$

For the DM noise separator of phase 3

$$\begin{aligned}\text{DMTR}^+ = {} & \frac{S_{41}}{(1+S_{11}+\Delta_1)} \cdot e^{j240^\circ} + \frac{S_{42}}{(1+S_{22}+\Delta_2)} \\ & \cdot e^{j120^\circ} + \frac{S_{43}}{(1+S_{33}+\Delta_3)}\end{aligned} \tag{45}$$

$$\begin{aligned}\text{DMTR}^- = {} & \frac{S_{41}}{(1+S_{11}+\Delta_1)} \cdot e^{-j240^\circ} + \frac{S_{42}}{(1+S_{22}+\Delta_2)} \\ & \cdot e^{-j120^\circ} + \frac{S_{43}}{(1+S_{33}+\Delta_3)}.\end{aligned} \tag{46}$$

As analyzed in the previous section, for DMTR_n^+ and DMTR_n^-, both magnitude and phase are important because the output of the DM noise separator is the vector sum of the positive and negative sequence voltage vectors. For a good DM noise separator, the magnitudes of both DMTR^+ and DMTR^- should be close to 0 dB and their phases should be same so the vector sum of the two sequences would not be changed at each frequency.

Based on (17)–(19), Fig. 6, and the symmetrical component theory, the DMRR^+ and DMRR^- for the CM noise separator and the CMRR for the DM noise separator can be derived similarly as follows.

For the CM noise separator

$$\begin{aligned}\text{DMRR}^+ = {} & \frac{S_{41}}{(1+S_{11}+\Delta_1)} + \frac{S_{42}}{(1+S_{22}+\Delta_2)} \cdot e^{-j120^\circ} \\ & + \frac{S_{43}}{(1+S_{33}+\Delta_3)} \cdot e^{-j240^\circ}\end{aligned} \tag{47}$$

$$\begin{aligned}\text{DMRR}^- = {} & \frac{S_{41}}{(1+S_{11}+\Delta_1)} + \frac{S_{42}}{(1+S_{22}+\Delta_2)} \cdot e^{j120^\circ} \\ & + \frac{S_{43}}{(1+S_{33}+\Delta_3)} \cdot e^{j240^\circ}.\end{aligned} \tag{48}$$

For the DM noise separator

$$\begin{aligned}\text{CMRR}_n = {} & \frac{S_{41}}{(1+S_{11}+\Delta_1)} + \frac{S_{42}}{(1+S_{22}+\Delta_2)} \\ & + \frac{S_{43}}{(1+S_{33}+\Delta_3)}.\end{aligned} \tag{49}$$

In (49), n is the port number from 1 to 3.

Equations [(25)–(27), (40)–(49)] are critical for three-phase noise-separator evaluation. For a three-phase noise separator, as long as the S-parameters are measured using a network analyzer, its performance can be evaluated through [(25)–(27), 40)–(49)]. In (25)–(27), if the second terms are much smaller than the first terms, the input impedances are independent from noise source impedances.

III. Design a Three-Phase Noise Separator

This section will first propose a function scheme for three-phase noise separators based on the theory developed in Section II-A. The circuit that can match the proposed function scheme is proposed and the design technique is explored.

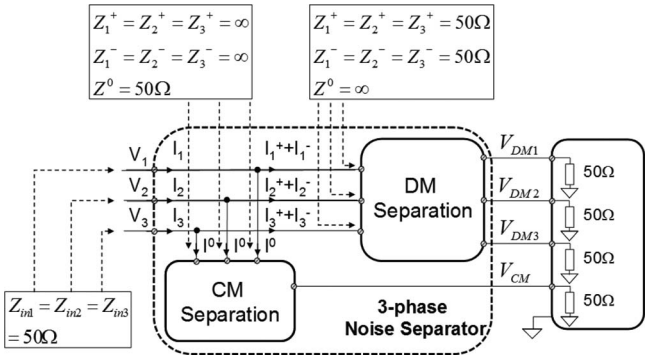

Fig. 8. Circuit structure for the proposed three-phase noise separator.

Finally, a three-phase noise separator is built with the proposed design technique.

A. Proposed Circuit Structure for Three-phase Noise Separators

Based on the analysis in previous section, CM noise is the zero-sequence noise and the DM noise is the sum of positive and negative sequence noises. A three-phase noise separator can be designed based on this principle following three steps. In the first step, a network that can separate positive and negative sequence noises from zero-sequence noise is developed. The network can also add positive sequence noise to negative sequence noise at its outputs. Furthermore, it can provide 50-Ω input impedances for positive and negative sequence noises and infinite input impedance for zero-sequence noise. In the second step, another network that can separate zero-sequence noise from positive and negative sequence noises is developed. The network should also provide 50-Ω input impedance for zero-sequence noise and infinite input impedance for positive and negative sequence noises. In the last step, the inputs of these two networks are connected in parallel. Based on the network theory, the combined network can achieve both noise separation function and 50-Ω input impedances for any noise. Fig. 8 shows this concept.

In Fig. 8, DM separation unit has 50-Ω input impedances Z_1^+, Z_2^+, Z_3^+ for positive and Z_1^-, Z_2^-, Z_3^- for negative sequence noise. Furthermore, it can conduct positive and negative sequence noises to a 50-Ω load without attenuation. On the other hand, the unit has very high impedance Z^0 for zero-sequence noise and does not conduct the zero-sequence noise to the 50-Ω load. The unit can, therefore, separate DM noise for each phase. The CM separation unit has a different story. It has 50-Ω impedance Z^0 for zero-sequence noise and can conduct the zero-sequence noise to a 50-Ω load without attenuation. At the same time, it has very high impedance, Z_1^+, Z_2^+, Z_3^+ for positive and Z_1^-, Z_2^-, Z_3^- for negative sequence noise. It does not conduct positive and negative sequence noises to the 50-Ω load. The CM separation unit can, thus, separate CM noise from DM noise. Because the DM separation unit has 50-Ω input impedance for positive and negative sequence noises and the CM separation unit has 50-Ω input impedance for zero-sequence noise, the combined input impedance of each phase is 50 Ω and it can be proved in

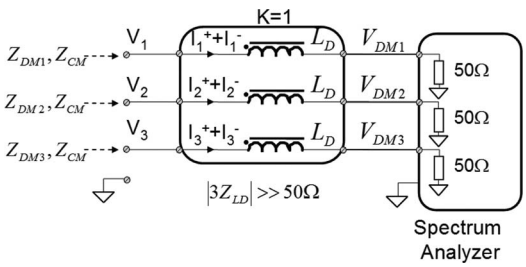

Fig. 9. Proposed circuit for the DM separation unit.

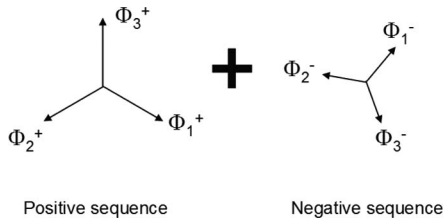

Fig. 10. Magnetic flux of positive and negative sequence noises was zero due to cancellation.

$$Z_{\text{in}\,n} = \frac{V_n}{I_n} = \frac{V^0 + V_n^+ + V_n^-}{I^0 + I_n^+ + I_n^-} = \frac{V^0 + V_n^+ + V_n^-}{(V^0/50\ \Omega) + (V_n^+/50\ \Omega) + (V_n^-/50\ \Omega)} = 50\ \Omega. \quad (50)$$

In (50), n is the input port number from 1 to 3.

B. Circuit Design for a Three-Phase Noise Separator

The circuit in Fig. 9 is proposed to achieve the function of the DM separation unit. Three inductors with an inductance L_D are closely coupled on one magnetic core with a coupling coefficient K equal to 1. They have high impedance $3Z_{LD}$ to CM (zero-sequence) noise within concerned frequency range. For positive and negative sequence noises, because their vector sum is zero and the coupled inductor has a balanced structure, the magnetic flux generated by each phase cancels each other inside the core as shown in (51) and Fig. 10. Ideally, for positive and negative sequence noises, the inductance and impedance are zero, so the input impedance of each phase is equal to the load impedance 50 Ω. As a result, the DM noise, which is the sum of positive and negative sequence noises, is conducted to the load without attenuation. For CM noise, the input impedance of each phase is given by (52) and the CMRR is given in (53). The inductor's CM impedance $|3Z_{LD}|$ should be much larger than 50 Ω to achieve a good CMRR and high CM input impedance

$$\sum_{n=1}^{3} \Phi_n^+ + \sum_{n=1}^{3} \Phi_n^- = L_D \left(\sum_{n=1}^{3} I_n^+ + \sum_{n=1}^{3} I_n^- \right) = 0 \quad (51)$$

$$Z_{\text{CM}} = 3Z_{LD} + 50 \quad (52)$$

$$\text{CMRR} = 20 \log \left| \frac{50}{3Z_{LD} + 50} \right|. \quad (53)$$

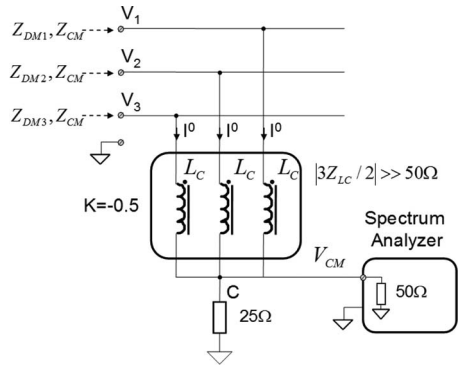

Fig. 11. Proposed circuit for the CM separation unit.

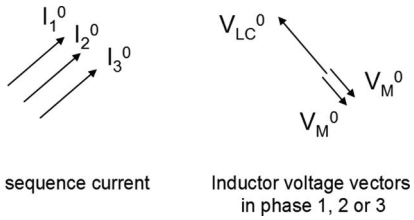

Fig. 12. Inductors have a zero voltage drop for zero-sequence noise.

In Fig. 9, if the inductor's coupling coefficient K is smaller than 1, there is leakage inductance on each phase. At high frequencies, the impedance could be significant so the input impedance will deviate from 50 Ω and the DM noise will be attenuated. Because of this, coupling coefficient K should, therefore, be as close to unity as possible.

The circuit in Fig. 11 is proposed to achieve the function of the CM separation unit. Each phase has an inductor with an inductance of L_C. The coupling coefficient between any two inductors is -0.5. Because the circuit has a balanced structure, the zero-sequence voltage excitation will generate zero-sequence currents only. For CM (zero-sequence) noise, the voltage vector sum $V_{\mathrm{CM\_LC}}$ of the induced voltage due to self inductance L_C and the induced voltage due to mutual inductance M is zero as shown in Fig. 12 and (54). Because of this, for CM noise, the inductor's impedance is zero. Three inputs are equivalently connected to the center point C. In Fig. 11, the total load impedance between the center point C and the ground is 50Ω/3. Three phases are in parallel for CM (zero-sequence) noise, so each phase equivalently has a 50-Ω load

$$V_{\mathrm{CM\_}LD} = V_{LC}^{0} - V_{M}^{0} - V_{M}^{0} = \left(j\omega L_D - j\omega\frac{L_D}{2} - j\omega\frac{L_D}{2}\right) \times I^{0} = 0. \quad (54)$$

For the inductor connected to phase1 in Fig. 11, the voltage responses to positive and negative sequence noises are shown in Fig. 13. In Fig. 13(a), the vector sum of the induced voltages V_{M2}^{+} and V_{M3}^{+} due to two mutual inductances has the same direction as that of the induced voltage V_{LC1}^{+} due to self-inductance and its amplitude is equal to 50% of V_{LC1}^{+}. The amplitude of the vector sum of the three vectors is, therefore, 150% of V_{LC1}^{+} and equal to V_1^{+}. As a result, the positive sequence noise current in the inductor is reduced by 1/3 compared with the case without mutual inductance. In Fig. 13(b), the negative sequence noise has the same story as the positive sequence noise. Because of this, the inductance is increased by 50% for positive and negative sequence noises as shown in (55) and (56). The other two inductors have the same story. Because the sum of positive and negative noises is DM noise, the inductance and DM impedance are also increased by 50% as shown in (57). The increased impedance $|3Z_{LC}/2|$ should be much larger than 50 Ω to achieve a high DM input impedance.

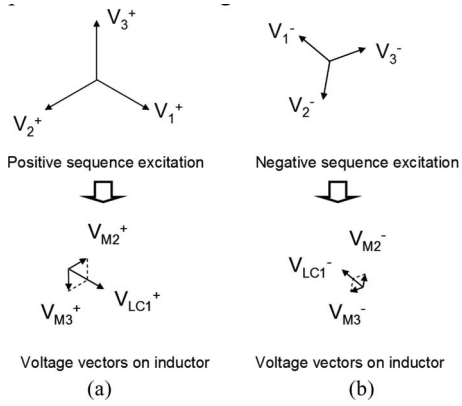

Fig. 13. Voltage vector diagram for phase-1 inductor with positive and negative sequence excitations.

Because three inductors are balanced, the voltage excitation at center point C in Fig. 11 is zero for positive and negative sequence excitations. The DMRR is, therefore, $-\infty$ dB. In a practical application, three coupled inductors should be as balance as possible to achieve good DMRRs

$$V_1^{+} = V_{LC1}^{+} + V_{M2}^{+} + V_{M3}^{+} = j\omega L_C I_1^{+} - j\omega\frac{L_C}{2} I_2^{+} - j\omega\frac{L_C}{2} I_3^{+} = j\omega\left(\frac{3}{2}L_C\right) I_1^{+} \quad (55)$$

$$V_1^{-} = j\omega\left(\frac{3}{2}L_C\right) I_1^{-} \quad (56)$$

$$Z_{\mathrm{DM1}} = \frac{V_1^{+} + V_1^{-}}{I_1^{+} + I_1^{-}} = j\omega\left(\frac{3}{2}L_C\right). \quad (57)$$

Based on the analysis in Section III-A, a three-phase noise separator can be developed by connecting the inputs of DM and CM separation units in parallel as shown in Fig. 14.

In Fig. 14, the DM separation unit has 50-Ω input impedance for the DM noise of each phase and high impedance for CM noise. It can conduct the DM noise of each phase to a 50-Ω load without attenuation. At the same time, it prevents the CM noise from reaching the 50-Ω load. On the other hand, the CM separation unit has 50-Ω input impedance for CM noise and high impedance for the DM noise of each phase. It can conduct the CM noise to a 50-Ω load without attenuation and prevent the DM noise from reaching the 50-Ω load. Because the inputs of DM and CM separation units are in parallel and any noise can be decoupled to CM and DM noises, the input impedance for

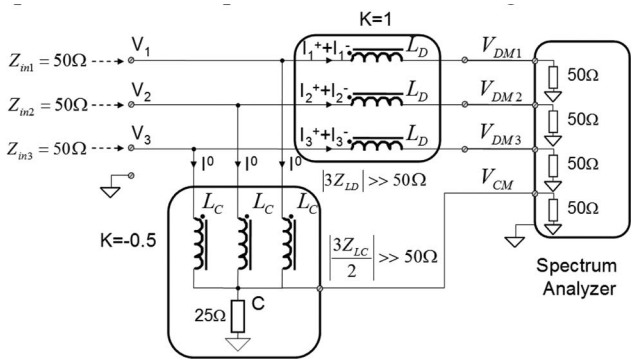

Fig. 14. Proposed three-phase noise separator.

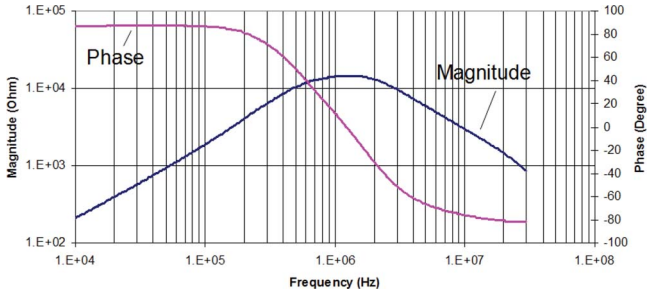

Fig. 15. Measured impedance Z_{LD} for the DM separation inductor.

any noise is, therefore, 50 Ω and at the same time, the separator can separate CM and DM noises for each phase.

C. Prototype Development

Based on the analysis in Section III-A and -B, to build a high-performance noise separator, the coupled inductors in the DM separation unit should meet the following conditions.

1) Inductance L_D should be big enough so that $|3Z_{LD}|$ has impedance much higher than 50 Ω within concerned frequency range and a good CMRR can be achieved.
2) Leakage inductance should be small enough so the inductor has DM impedance much smaller than the 50-Ω load and a good DMTR can be achieved.

A high-permeability ferrite toriodal core, ZJ42206TC (J material from Magnetics Inc.), is used for the inductor design. A 30-turn trifilar winding structure is employed to achieve high coupling coefficient. For trifilar winding structure, three wires are almost at the same position, so the leakage energy is only stored in the air gap between three wires. A low leakage inductance is achieved. The measured inductance is shown in Fig. 15.

The measured impedance curves in Fig. 15 shows that the CM inductance is 3 mH with an equivalent CM parallel winding capacitance of 5.67 pF and an equivalent CM parallel resistance of 14.5 kΩ. At frequencies higher than 1.2 MHz, CM impedance is determined by the winding capacitance. The impedance $|3Z_{LD}|$ is much larger than 50 Ω. To further improve CMRR at 10 kHz, a bigger inductance is preferred by increasing the number of turns for the trifilar winding as described in (53). However, this may sacrifice inductor's HF impedance because more number of turns may result in a larger CM winding capacitance. A good

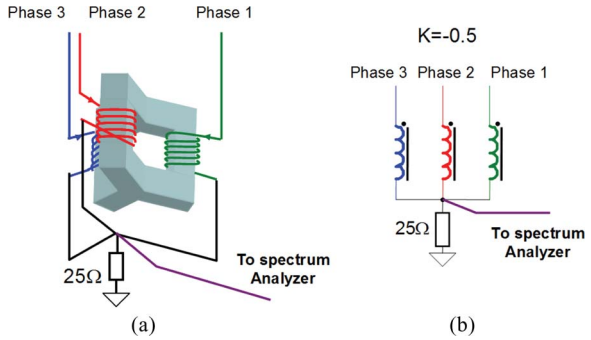

Fig. 16. Coupled three-phase inductor with a coupling coefficient of −0.5. (a) Inductor structure 1 and (b) equivalent circuit.

solution is to design a noise separator for low-frequency range (10–150 kHz) with a larger inductance L_D and a noise separator for HF range (150 kHz to 30 MHz) with a smaller inductance L_D. Because the objective of this paper is to present the theory developed to characterize three-phase noise separators and the circuit and component structures proposed to build a three-phase noise separator, only one noise separator operating from 150 kHz to 30 MHz will be investigated here.

The measured coupling coefficient between any two windings is 0.99995 and the leakage inductance for positive and negative sequence noises is 174 nH. At 30 MHz, it has an impedance of 33 Ω for DM noise, so it is not negligible compared with 50-Ω load. To reduce the effects of leakage inductance, the parasitic capacitance between three windings can be used to cancel the effects of leakage inductance based on the transmission line transformer theory [2]. To achieve this, for positive and negative sequence noises, the characteristic impedance of the three-conductor transmission line should be close to 50 Ω. The characteristic impedance can be designed by adjusting the space between three wires. The measured characteristic impedance for positive and negative sequence noises is 43.3 Ω, which is close to 50 Ω, so the effect of leakage inductance is reduced.

For CM separation unit, the coupled inductors should meet the following conditions.

1) L_C should be big enough so that $|3Z_{LC}/2|$ has impedance much higher than 50 Ω within concerned frequency range. This helps the noise separator to achieve 50-Ω input impedance for DM noise.
2) Three inductors should be as balance as possible. The coupling coefficient between two windings should be as close to unity as possible. The impedance of the leakage inductance between two windings should be much smaller than 50 Ω. These conditions guarantee that the noise separator has a good CMTR and DMRR.

There are two methods to build the coupled inductors for CM separation unit. The first method is using a core with three symmetrical legs as shown in Fig. 16(a). In Fig. 16(a), the coupling coefficient between any two windings is −0.5. Fig. 16(b) shows its equivalent circuit. This method is straightforward but it is difficult to make the core. Using planar E shapes cores is also not a good method because the reluctances of three inductors are not balanced. The second method is using three identical

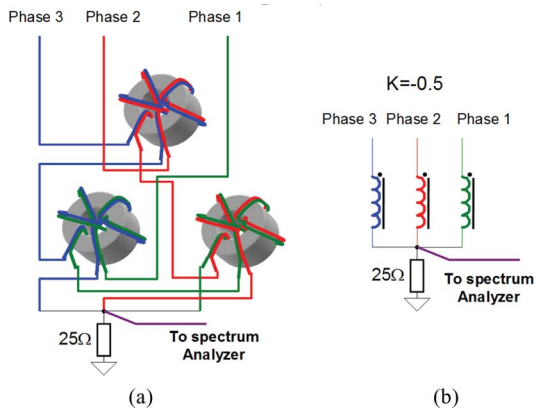

Fig. 17. Coupled three-phase inductors with a coupling coefficient of −0.5. (a) Inductor structure 2 and (b) equivalent circuit.

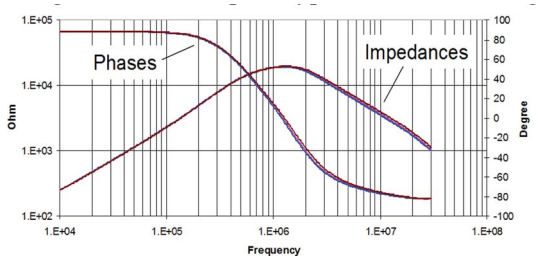

Fig. 18. Measured impedance Z_{LC} for the CM separation inductors.

inductors as shown in Fig. 17(a). In Fig. 17(a), each inductor has two windings closely coupled with a coupling coefficient of −1. Three inductors are connected in such a way that the inductor L_C on each phase in Fig. 14 includes two series windings on two different inductors and these two windings are inversely coupled to the other two windings on the inductors as shown in Fig. 17(a). Because the three inductors are identical, the coupling coefficient between any two L_Cs is −0.5. Fig. 17(b) shows its equivalent circuit. The second method is easier than the first method so it is used in the experiment. The same cores as used in DM separation unit are used here for inductor design. Each inductor has a 33-turn bifilar winding structure.

The measured impedances of three inductors are shown in Fig. 18. It is shown that the impedances of three inductors are almost the same. $|3Z_{LC}/2|$ is around 375 Ω at 10 kHz which is much larger than 50 Ω. To further increase $|3Z_{LC}/2|$, more number of turns is needed for the inductor. Similar to the solution of L_D, two sets of inductors can be designed to solve this problem. One targets 10–150 kHz and the other targets 150 kHz–30 MHz. This paper will discuss the separator operating from 150 kHz to 30 MHz only. The measured coupling coefficient between two windings is around 0.99997, so the leakage inductance is small and the coupling coefficient between two L_Cs is very close to −0.5. The inductors, therefore, meet the conditions defined previously.

The CM and DM separation units are connected together as shown in Fig. 14. The final prototype is shown in Fig. 19.

Fig. 19. Three-phase noise separator prototype.

IV. Experimental Results

The experiment is carried out by two steps. Because the noise separator includes CM, DM1 (phase1 DM), DM2 (phase2 DM), and DM3 (phase3 DM) separation parts, in the first step, the S-parameters of each part are measured separately. Based on the measurement results, the noise separator is evaluated using the theory developed in Section II. The input impedance of each port, CMTR, CMRR, DMTR^+, DMRR^+, DMTR^-, and DMRR^- are all evaluated. In the second step, the noise separator is used in a practical three-phase power electronics circuit for noise measurement.

A. Evaluation of the Noise Separator

The S-parameters for CM, DM1, DM2, and DM3 separation parts are measured separately. Due to the frequency range limitation of the network analyzer (Agilent E5070B), the S-parameters are measured from 300 kHz to 30 MHz. When the S-parameter of one separation part is measured, the output ports of the other parts are terminated with 50-Ω resistances so the reflection coefficients of those ports are zero and they have no effects on the measurement. For example, when the S-parameter of the DM1 separation part is measured, the output ports of DM2, DM3, and CM are terminated with 50-Ω resistances. The signal-flow graph of the DM1 separation part is given by Fig. 6. DM2, DM3, and CM parts are measured in the same way as DM1 and all of them can be characterized with the signal-flow graph in Fig. 6. After the S-parameters are measured, the noise separator is evaluated using the theory developed in Section II. Input impedances, CMTR, CMRR, DMTR^+, DMRR^+, DMTR^-, and DMRR^- are derived and shown in Figs. 20–25.

Fig. 20(a) and (b) shows the magnitude and phase for one of the three input impedances of the noise separator with different noise source impedances connected to the other two input ports. It is shown that the input impedance is within 45–55 Ω and the phase is between −20° and –10°, so the input impedance is close to real 50 Ω and it almost independent from the noise source impedance within measured frequency range. The other two input impedance curves are almost the same as the one shown in Fig. 20(a) and (b). So all the inputs of the noise separator can provide real 50-Ω resistive input impedances and they are noise source impedance independent.

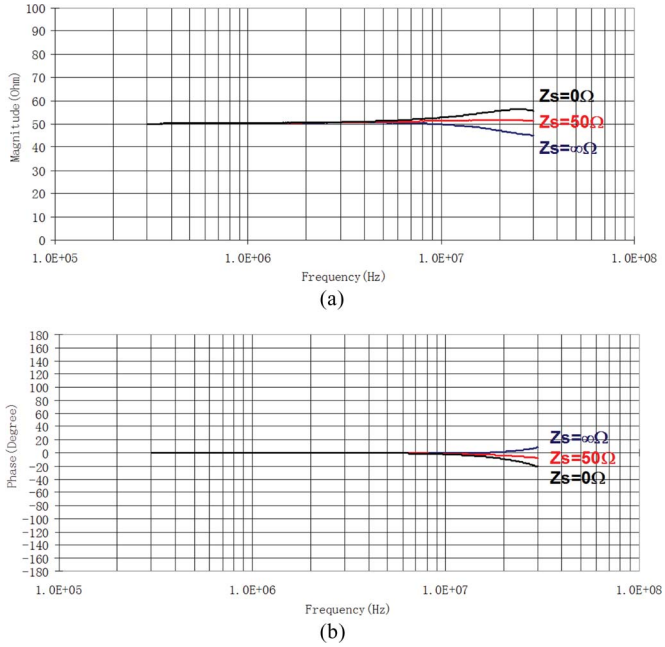

Fig. 20. Input impedances of the noise separator when noise source impedance is 0 Ω, 50 Ω, and ∞ Ω. (a) Magnitude and (b) phase.

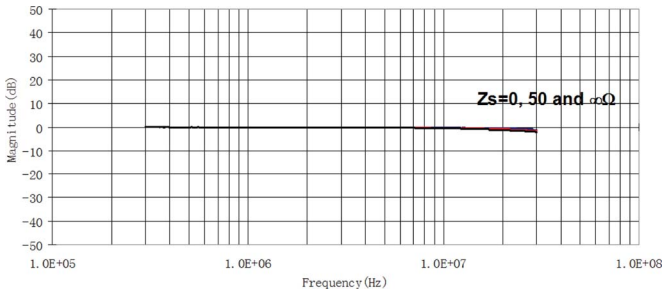

Fig. 21. CMTR of the noise separator when noise source impedance is 0 Ω, 50 Ω, and ∞ Ω.

Fig. 21 shows the CMTR of the CM separation of the noise separator. The CMTR is very close to ideal 0 dB. The phase is not shown here since it is not important for CMTR.

Fig. 22 shows the $DMRR^+$ and $DMRR^-$ of CM separation with different noise source impedances. It is shown that $DMRR^+$ and $DMRR^-$ are independent from noise source impedances because three curves are almost the same. As analyzed in the previous section, $DMRR^+$ and $DMRR^-$ should be as small as possible. In the figures, both $DMRR^+$ and $DMRR^-$ are smaller than -40 dB, so they are pretty good.

Figs. 23 and 24 show the magnitude and phase of the $DMTR^+$ and $DMTR^-$ of the DM1 noise separation under different noise source impedance conditions. The $DMTR^+$ and $DMTR^-$ of the DM2 and DM3 noise separations are almost the same as those of DM1 noise separation. Fig. 23 shows that the both $DMTR^+$ and $DMTR^-$ are very close to 0 dB. Fig. 24 shows that $DMTR^+$ and $DMTR^-$ have almost the same phase angle. Because of these, the positive and negative sequence noises at each frequency can be combined into DM noise at the output of the noise separator without any changes.

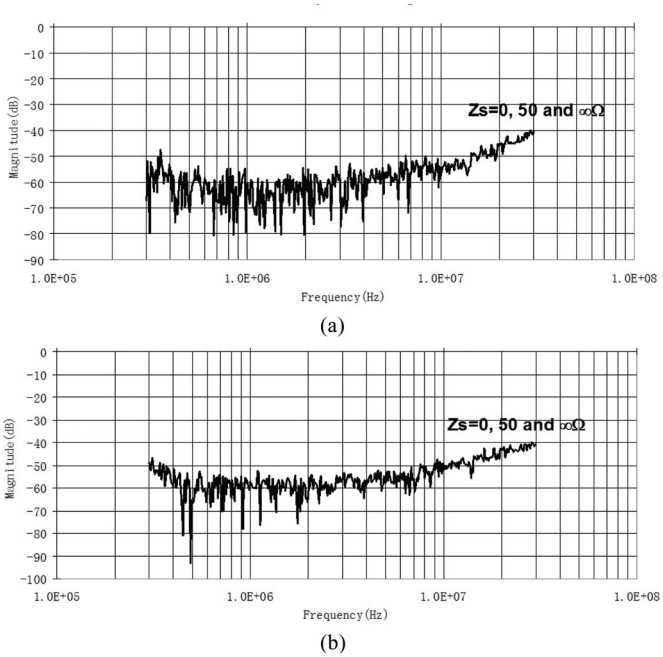

Fig. 22. $DMRR^+$ and $DMRR^-$ of the CM noise separator when noise source impedance is 0 Ω, 50 Ω, and ∞ Ω. (a) $DMRR^+$ and (b) $DMRR^-$.

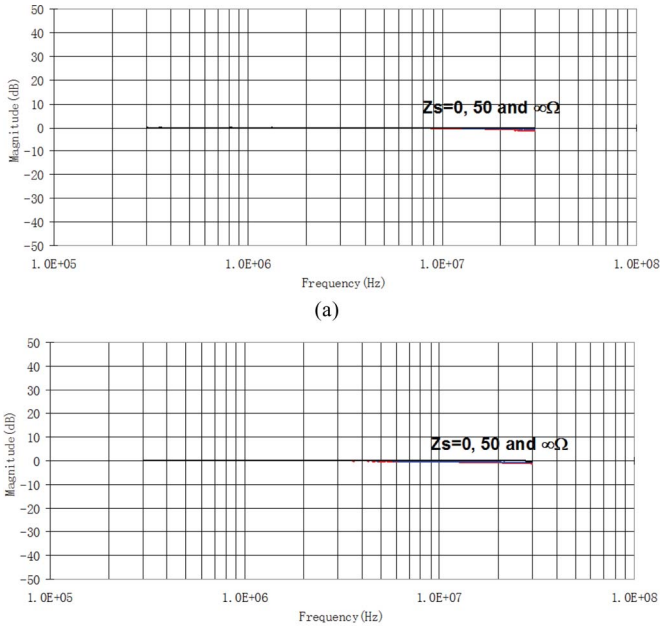

Fig. 23. Magnitudes of the $DMTR^+$ and $DMTR^-$ of the DM1 noise separator when noise source impedance is 0 Ω, 50 Ω, and ∞ Ω. (a) $DMTR^+$ and (b) $DMTR^-$.

Fig. 25 shows the CMRR of the DM1 noise separation under different noise source impedance conditions. The CMRR of the DM2 and DM3 noise separations is almost the same as that of DM1 noise separation.

The CMRR should be as small as possible. Fig. 25 shows that the CMRR is smaller than -34 dB within measured frequency range, so it is good.

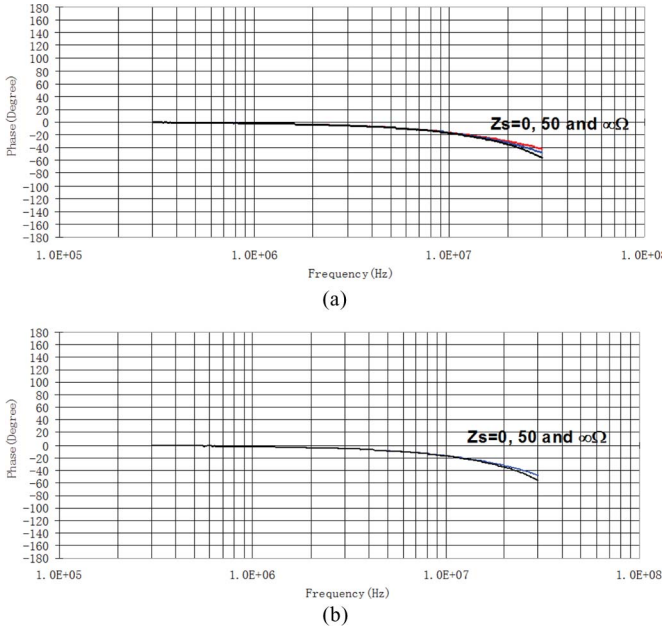

Fig. 24. Phases of the $DMTR^{+}$ and $DMTR^{-}$ of the DM1 noise separator when noise source impedance is 0 Ω, 50 Ω, and ∞ Ω. (a) $DMTR^{+}$ and (b) $DMTR^{-}$.

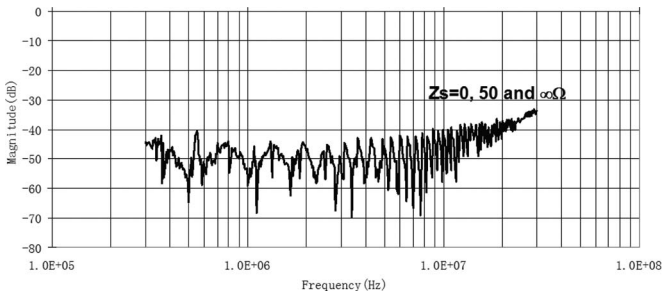

Fig. 25. CMRR of DM1 noise separation when noise source impedance is 0 Ω, 50 Ω, and ∞ Ω.

B. EMI Noise Measurement With the Noise Separator

The noise separator was used to measure the DM and CM noises for a practical three-phase power electronics system shown in Fig. 26. In Fig. 26, a three-phase 60-Hz voltage source feeds power to a three-phase insulated gate bipolar transistor (IGBT) rectifier. The load of the rectifier is a 225-Ω resistor and the dc bus has a voltage of 150 V. Three-phase LISNs are inserted between the three-phase voltage source and the three-phase IGBT rectifier. The outputs of the LISN are directly connected to the inputs of the three-phase noise separator. The output of the noise separator is connected to a spectrum analyzer. The unconnected outputs of the noise separator are terminated by 50-Ω terminators. The CM and DM peak noises are measured from 150 kHz to 30 MHz with a resolution bandwidth of 9 kHz. The measurement results are shown in Figs. 27 and 28.

In Figs. 27 and 28, it is shown that DM noise is dominant from 150 kHz to 4 MHz, and from 5 to 22 MHz. From 4 to 5 MHz and from 22 to 30 MHz, CM noise is comparable with DM noise. Based on the measured DM, CM noise, and the correspondent EMI standards, DM and CM EMI filters can be easily optimized with higher power densities and lower cost than the designs without the help of noise separators.

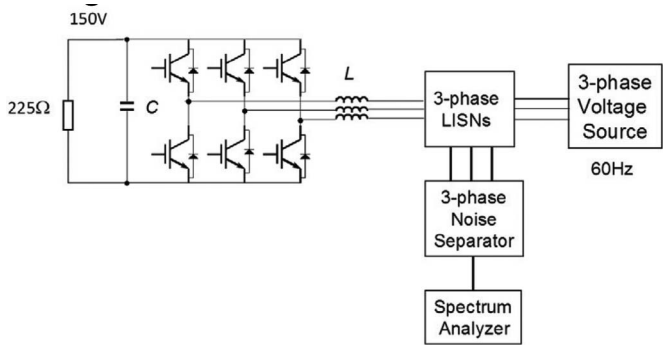

Fig. 26. Setup for three-phase EMI measurement with the help of a three-phase noise separator.

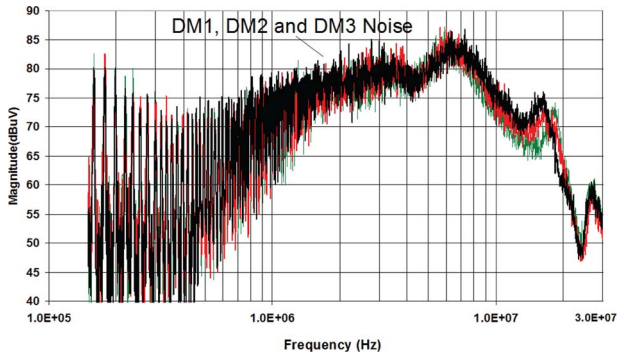

Fig. 27. Measured three-phase DM noise using the proposed three-phase noise separator.

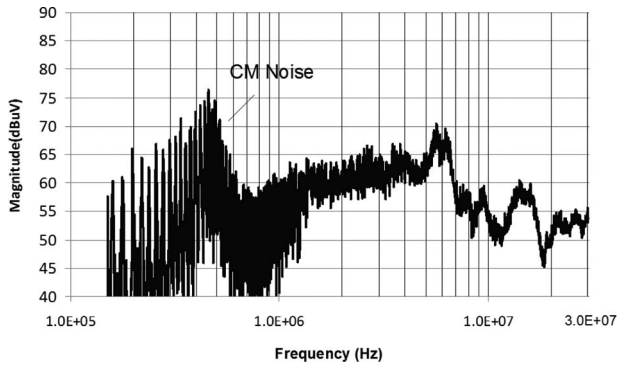

Fig. 28. Measured three-phase CM noise using the proposed three-phase noise separator.

V. Conclusion

In this paper, three-phase noise is first analyzed using symmetrical component theory. CM noise is a zero-sequence noise and DM noise is the sum of positive and negative sequence noises. The S-parameter model is developed for both ideal and practical three-phase noise separators based on symmetrical component theory and network theory. The critical parameters such as input impedances, CMTR, $DMTR^{+}$, $DMTR^{-}$, CMRR,

$DMRR^+$ and $DMRR^-$ are all derived using S-parameters. With the developed theory in this paper, a three-phase noise separator can be easily and correctly analyzed and evaluated by measuring its network parameters. A function scheme and a circuit structure for three-phase noise separators are proposed based on the developed theory. The technique to design the coupled inductors in DM and CM separation units for high-performance three-phase noise separators is explored. A three-phase noise separator prototype is finally built based on the developed technique. The prototype was measured and evaluated using the theory in this paper. The proposed three-phase noise separator is very useful in optimizing the EMI filter design and improving the power densities for three-phase power electronics systems.

REFERENCES

[1] Y. Y. Maillet, R. Lai, S. Wang, F. Wang, R. Burgos, and D. Boroyevich, "High-density EMI filter design for DC-fed motor drives," *IEEE Trans. Power Electron.*, vol. 25, no. 5, pp. 1163–1172, May 2010.

[2] S. Wang, F. Lee, and W. G. Odendaal, "Characterization, evaluation and design of noise separator for conducted EMI noise diagnosis," *IEEE Trans. Power Electron.*, vol. 20, no. 4, pp. 974–982, Jul. 2005.

[3] D. Zhang, D.Y. Chen, and D. Sable, "A new method to characterize EMI filters," in *Proc. IEEE Appl. Power Electron. Conf. Expo.*, Anaheim, CA, Feb. 15–19, 1998, pp. 929–933.

[4] R. Anderson, "Test and measurement application note 95-1 S-parameters techniques," Hewlett-Packard, Palo Alto, CA, 1997.

[5] D. M. Pozar, *Microwave Engineering*. Hoboken, NJ: Wiley, 1998.

[6] N. Balabanian and T. Bickart, *Linear Network Theory: Analysis, Properties, Design and Synthesis*. Beaverton, OR: Matrix, 1981.

[7] W. Medley, *Microwave and RF Circuits: Analysis, Synthesis, and Design*. Norwood, MA: Artech House, 1993.

[8] *Agilent AN154 S-Parameters Design Application Note*. Agilent Technologies, Santa Clara, CA, 2000.

[9] P. S. Chen and Y. S. Lai, "Effective EMI filter design method for three-phase inverter based upon software noise separation," *IEEE Trans. Power Electron.*, vol. PP, no. 99, p. 1, Jul. 2010.

[10] C. R. Paul and K. B. Hardin, "Diagnosis and reduction of conducted noise emissions," *IEEE Trans., Electromagn. Compat.*, vol. 30, no. 4, pp. 553–560, Nov. 1988.

[11] H.-L. Su and K.-H. Lin, "Computer-aided design of power line filters with a low cost common and differential-mode noise diagnostic circuit," in *Proc. IEEE Int. Symp. Electromagn. Compat.*, Montreal, Canada, Aug. 13–17, 2001, pp. 511–516.

[12] M. C. Caponet, F. Profumo, L. Ferraris, A. Bertoz, and D. Marzella, "Common and differential mode noise separation: comparison of two different approaches," in *Proc. IEEE Power Electron. Spec. Conf.*, Vancouver, Canada, Jun. 17–21, 2001, pp. 1383–1388.

[13] M. C. Caponet and F. Profumo, "Devices for the separation of the common and differential mode noise: design and realization," in *Proc. IEEE Appl. Power Electron. Conf. Expo.*, Dallas, TX, Mar. 10–14, 2002, pp. 100–105.

[14] M. L. Heldwein, J. Biela, H. Ertl, T. Nussbaumer, and J. W. Kolar, "Novel three-phase CM/DM conducted emission separator," *IEEE Trans. Ind. Electron.*, vol. 56, no. 9, pp. 3693–3703, Sep. 2009.

[15] M. J. Nave, "A novel differential mode rejection network for conducted emissions diagnostics," in *Proc. IEEE Nat. Symp. Electromagn. Compat.*, Denver, CO, May 23–25, 1989, pp. 223–227.

[16] G. Ting, D. Y. Chen, and F. C. Lee, "Separation of the common-mode and differential-mode conducted EMI noise," *IEEE Trans. Power Electron.*, vol. 11, no. 3, pp. 480–488, May 1996.

[17] S. K. Yak and N. C. Sum, "Diagnosis of conducted interference with discrimination network," in *Proc. IEEE Int. Conf. Power Electron. Drive Syst.*, Singapore, Feb. 21–24, 1995, pp. 433–437.

[18] Y.-K. Lo, H.-J. Chiu, and T.-H. Song, "A software-based CM and DM measurement system for the conducted EMI," *IEEE Trans. Ind. Electron.*, vol. 47, no. 4, pp. 977–978, Aug. 2000.

[19] M. J. Nave, *Power Line Filter Design for Switched-Mode Power Supply*. New York: Van Nostrand, 1991.

[20] A. Nagel and R. W. De Donker, "Separating common mode and differential mode noise in EMI measurements," in *Proc. Eur. Power Electron. Drives (EPE) Conf.*, Lousanne, 1999, pp. 1–8.

[21] J. Sevick, *Transmission Line Transformers*. Newington, CT: Am. Radio Relay League, 1987.

[22] G. Ting, *Separation of the Common-Mode and the Differential-Mode Conducted Electromagnetic Interference Noise*, Master thesis, Virginia Tech, Blacksburg, VA, 1994.

Shuo Wang (S'03–M'06–SM'07) received the B.S.E.E. degree from Southwest Jiaotong University, Chengdu, China, in 1994, the M.S.E.E. degree from Zhejiang University, Hangzhou, China, in 1997, and the Ph.D. degree from the Center for Power Electronics Systems (CPES), Virginia Polytechnic Institute and State University, Blacksburg, in 2005.

Since 2010, he has been with the Department of Electrical and Computer Engineering, University of Texas at San Antonio. From 2009 to 2010, he was with the Electrical Power Systems Group, GE Aviation Systems, Vandalia, OH. From 2005 to 2009, he was with CPES at Virginia Tech. He is the holder of five U.S. patents and has two others pending. He has published more than 80 journal and conference papers. His research interests include electromagnetic interference/electromagnetic compatibility in power electronics systems, high-density power conversion, three-phase power conversion and inversion, motor drives, generator control, power systems, and microgrid.

Dr. Wang is an Associate Editor for the IEEE TRANSACTIONS ON INDUSTRY APPLICATIONS. He was the recipient of the 2005 Best Transactions Paper Award from the IEEE TRANSACTIONS ON POWER ELECTRONICS, and the William M. Portnoy Award for the best paper presented at the IEEE Industry Applications Society Annual Conference in 2004.

Fang Luo (S'06–M'11) was born in Wuhan, Hubei, China. He received the Bachelor's and Ph.D. degrees from the Huazhong University of Science and Technology, Wuhan, China, in 2003 and 2010, respectively.

Since 2007, he has been a visiting scholar at the Center for Power Electronics Systems (CPES), Virginia Tech, Blacksburg, supported by Chinese Scholarship Council and CPES. His experience in power electronics includes research and development on uninterrupted power supply (UPS) systems, battery monitoring and management system, and dc power distribution network protection. His current topic is high-density electromagnetic interference (EMI) filtering solution and passive EMI filter integration in motor drive systems.

Fred C. Lee (S'72–M'74–SM'87–F'90) received the B.S. degree in electrical engineering from the National Cheng Kung University, Tainan, Taiwan, in 1968, and the M.S. and Ph.D. degrees in electrical engineering from Duke University, Durham, NC, in 1972 and 1974, respectively.

He is currently a University Distinguished Professor at Virginia Polytechnic Institute and State University (Virginia Tech), Blacksburg. He is the Founder and Director of the Center for Power Electronics Systems, a National Science Foundation engineering research center. He had also supervised 69 Ph.D. and 76 master students at Virginia Tech. He holds 61 U.S. patents. He is the author or coauthor of 229 journal articles and more than 570 refereed technical papers. His current research interests include high-frequency power conversion, distributed power systems, renewable energy, power quality, high-density electronics packaging and integration, and modeling and control.

Dr. Lee is a recipient of the William E. Newell Power Electronics Award in 1989 and the Arthur E. Fury Award for Leadership and Innovation in 1998. During 1993–1994, he was the President of the IEEE Power Electronics Society.

Dr. Lee is a member of National Academy of Engineering.